



# Hydroclimate variability in the United States continental interior during the early Eocene Climatic Optimum

Amy L. Elson<sup>a,\*</sup>, Megan Rohrsen<sup>b</sup>, John Marshall<sup>a</sup>, Gordon N. Inglis<sup>a</sup>, Jessica H. Whiteside<sup>a</sup>

<sup>a</sup> School of Ocean and Earth Science, University of Southampton, National Oceanography Centre Southampton, UK

<sup>b</sup> Geology and Environmental Sciences, Central Michigan University, USA

## ARTICLE INFO

Editor: Shucheng Xie

### Keywords:

Eocene  
Green River Formation  
EECO  
Hydrogen cycle  
Compound-specific hydrogen isotope analysis  
Lacustrine

## ABSTRACT

The early Eocene (56.0 to 47.8 million years ago) was punctuated by a series of transient episodes of rapid global warming superimposed on the long-term early Cenozoic warming trend, culminating in the early Eocene Climatic Optimum (EECO; 53.3 to 49.1 million years ago). Details of the hydroclimate regime operating during the EECO are poorly constrained, especially for continental interior sites. The Green River Formation (GRF) of Utah and Colorado was deposited in a suite of large, unusually productive lakes that offer an ideal opportunity to study the hydrological response to warming. Here we report the hydrogen isotopic composition ( $\delta^2\text{H}$ ) of leaf wax (long-chain *n*-alkanes) and algal (phytane) lipids preserved in the organic-rich Mahogany Zone (49.3 to 48.7 Ma) and use these data to reconstruct precipitation and lake water  $\delta^2\text{H}$  records, respectively. We observe large inter-site variations in algal and leaf wax  $\delta^2\text{H}$  values ( $\sim 50$  to 75‰), suggesting that additional local controls influence precipitation and/or lake water  $\delta^2\text{H}$  (e.g., salinity). Intriguingly, leaf wax and algal lipid  $\delta^2\text{H}$  values show little variation through the Mahogany Zone, implying a relatively stable hydrological regime during the latter phase of the EECO. This contrasts with the more variable hydrological regime that prevailed during early Eocene hyperthermals. Unlike the EECO, the early Eocene hyperthermals in the Uinta region do not coincide with the deposition of organic-rich sediments. This suggests that a stable hydrological regime during the EECO may enable the preservation of organic matter within continental-interior lake systems, potentially leading to an important negative climate feedback during the early Eocene and other greenhouse climates.

## 1. Introduction

The Green River Formation (GRF) was deposited between  $\sim 53$  and 44 million years ago (Ma) and represents a series of intermittently interconnected terminal continental-interior basins that extended across north-eastern Utah, north-western Colorado, and south-western Wyoming (Bradley, 1929; Tissot et al., 1978; Dyni, 1987; Smith et al., 2008, 2010) (Fig. 1). Lake Uinta was deposited in the Uinta Basin (north-eastern Utah) and is characterized by at least three hypersaline intervals (Vanden Berg and Birgenheier, 2017). The first of these coincides with the richest interval of organic carbon (OC) content in the Green River Formation, the Mahogany Zone (MZ). Deposited over  $\sim 400$  thousand-years (kyr), the MZ comprises sediments deposited in the deepest part of the paleo-lake (Tissot et al., 1978). This unusually organic-rich section is found throughout the basin and contains a thin (0.5 meter; m) marker bed of peak total organic carbon (TOC; 43 weight percent; wt %; Whiteside and Van Keuren, 2009), referred to as the Mahogany Bed

marker.

The MZ was deposited towards the end of the early Eocene Climatic Optimum (EECO; 53.3 to 49.1 Ma) and is constrained by radioisotopic dating ( $49.32 \pm 0.30$  to  $48.66 \pm 0.23$  Ma; Smith et al., 2008, 2010). The EECO was an interval of sustained global warmth, with global surface temperatures reaching  $\sim 10$ – $16$  °C above pre-industrial levels (Zachos et al., 2001; Inglis et al., 2020). The EECO is also characterized by an intensified hydrological cycle (Carmichael et al., 2016) with evidence for enhanced rainfall in high-latitudes (Carmichael et al., 2016; Inglis et al., 2022). However, the hydrological response within the low to mid-latitude continental interiors has been assessed in only a few studies (Hyland and Sheldon, 2013; Carmichael et al., 2016). A better understanding of hydrological cycle perturbations during the early Eocene could provide important insights into a range of biogeochemical processes, including soil erosion rates, methane cycling and organic carbon burial (Carmichael et al., 2017 and references therein). These processes may have acted as positive or negative feedbacks to global warming and

\* Corresponding author.

E-mail address: [ale1u16@soton.ac.uk](mailto:ale1u16@soton.ac.uk) (A.L. Elson).

<https://doi.org/10.1016/j.palaeo.2022.110959>

Received 27 April 2021; Received in revised form 20 March 2022; Accepted 24 March 2022

Available online 27 March 2022

0031-0182/© 2022 The Authors. Published by Elsevier B.V. This is an open access article under the CC BY license (<http://creativecommons.org/licenses/by/4.0/>).

thus, may have played an important role in early Cenozoic greenhouse conditions. However, understanding these processes requires better constraints on the hydrological cycle of these large early Eocene lakes.

Here we determine compound-specific hydrogen isotope ( $\delta^2\text{H}$ ) values in leaf waxes and algal lipids to reconstruct changes in the hydrological cycle over the mid-latitudes during the deposition of the MZ. In modern settings, leaf waxes record the  $\delta^2\text{H}$  of the source water from the surrounding vegetative environment, whereas phytane is commonly derived from autotrophic aquatic microorganisms and provides insights into the  $\delta^2\text{H}$  value of lake water (Volkman et al., 1998; Eglinton and Eglinton, 2008; Sachse et al., 2004, 2012). We use lipid  $\delta^2\text{H}$  values to infer changes in the  $\delta^2\text{H}$  value of precipitation through the latest EECO and post-EECO interval ( $\sim 49.3$  to  $48.7$  Ma) and assess the stability of the hydrological cycle during this event. We also explore the role of the hydrological cycle in the deposition of the organic-rich Mahogany Zone during the termination of the EECO.

## 2. Background and methods

### 2.1. Site description

Continual industry interest in the oil shales of the Green River Formation has resulted in numerous boreholes, particularly in the Uinta Basin. We sampled a centre to margin transect of the profundal zone through three Mahogany Zone sections (Fig. 1). The main facies represented are continuous parallel- to undulose laminated mudstone with little bioturbation. Drilled by TOSCO, the Utah State 1 core represents a deep, basal zone of the Uinta Basin (reported as  $40.010576^\circ\text{N}$ ,  $109.511638^\circ\text{W}$ ). The P-4 Chevron White Shale Project core (P-4) was drilled in the eastern section of the Uinta basin, targeting a basin-margin lacustrine environment ( $39.931419^\circ\text{N}$ ,  $109.134227^\circ\text{W}$ ). Drilled by the Utah Geological Survey, the Skyline 16 core represents a proximal basin-margin, lacustrine setting and contains a relatively condensed section of the Mahogany Zone ( $39.870658^\circ\text{N}$ ,  $109.112281^\circ\text{W}$ ).

### 2.2. Age model

The Green River Formation is punctuated by numerous tuff layers from the northeastern Absaroka Volcanic Province. Two dated tuff horizons - the Curly and Wavy tuffs ( $49.32 \pm 0.33$  Ma and  $48.66 \pm 0.27$  Ma respectively; Smith et al., 2008) – are found below and above the Mahogany Zone of the P-4 drill core, respectively. These tuff layers have been dated with  $^{40}\text{Ar}/^{39}\text{Ar}$ , measured on single crystal analysis of biotite (Smith et al., 2008) and used to develop an age model for the P-4, Skyline 16, and Utah State 1 Mahogany Zone sections. Detailed sedimentological analysis supports a nearly constant accumulation rate of  $100\text{--}200 \mu\text{m}/\text{yr}$  (Smith et al., 2008; Whiteside and Van Keuren, 2009; Walters et al., 2020).

### 2.3. Organic geochemistry

Rock plugs through the Mahogany Zone from Utah State 1, P-4 and Skyline 16 (2274–2376 ft., 683–785 ft. and 430–513 ft. respectively) were removed with a water-cooled drill press (Delta DP300L) and powdered by agate mortar and pestle. Molecular extraction and fractionation were conducted at the University of Southampton. Total lipid extracts (TLE) were isolated from powdered rock using a Thermo 350 Accelerated Solvent Extractor with the following program: preheat = 5 min; heat = 5 min; static = 5 min; pressure = 1500 psi; flush = 70%, purge = 300 s.; cycles = 3; solvent = dichloromethane:methanol (9:1, v/v). Solvent extracts were evaporated using a Genevac EZ-2 vacuum centrifuge and subsequently fractionated using silica gel columns. The TLE was eluted with hexane, hexane:dichloromethane (DCM) (4:1, v/v), and DCM:methanol (MeOH) (1:1, v/v), yielding the aliphatic, aromatic and polar fractions, respectively. Activated copper was added to each fraction to remove elemental sulphur.

Biomarker identification was performed using a Thermo Trace 1310 Gas Chromatograph (GC) coupled to a Thermo TSQ8000 Triple Quadrupole Mass Spectrometer (MS). The GC used a DB-5 column (30 m  $\times$

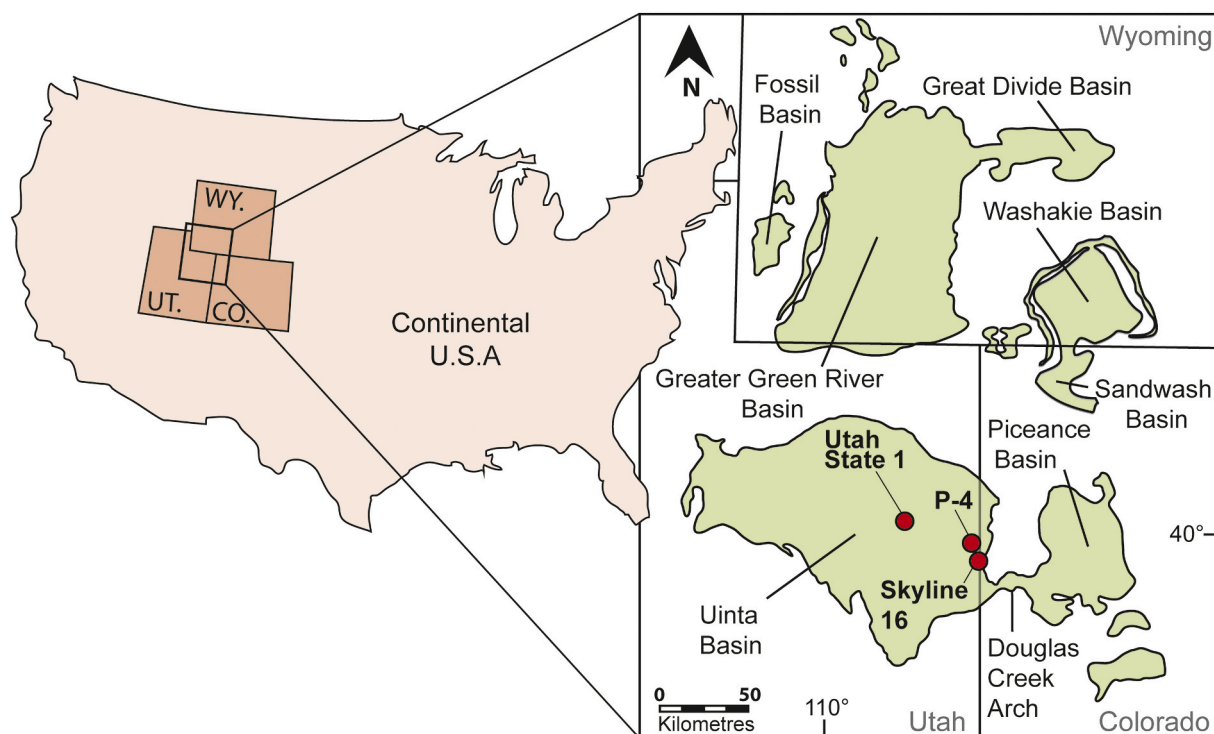


**Fig. 1.** The lateral extent of the Green River Formation spanning north-east Utah, north-west Colorado and southern Wyoming (Grande, 1984). This study focused on the southern Uinta Basin in Utah, through three Mahogany Zone sections varying in proximity to the paleoshore. Utah State 1 was in the basin-centre during the deposition of the Mahogany Zone, whereas P-4 and Skyline 16 represent the basin-margin during this time. Locations of the cores are indicated in red circles. (For interpretation of the references to colour in this figure legend, the reader is referred to the web version of this article.)

0.25 mm i.d., 0.25- $\mu\text{m}$  film thickness) with the following oven program: 40 °C (held for 2 min), increased at a rate of 6 °C/min to 310 °C, and then held for 20 min. Compound identification of *n*-alkanes and pristane/phytane was made using mass spectra and comparison with an in-house reference oil (North Sea Oil-1).

Compound-specific hydrogen isotope analysis was conducted using a Thermo Scientific Trace 1310 GC with a DB-5 column (30 m  $\times$  0.25 i.d., 0.25- $\mu\text{m}$  film thickness) coupled to a Delta V Plus Isotope Ratio Mass Spectrometer via a Thermo GC Isolink and ConFlo IV. Samples were injected splitless and the GC program was as follows: 40° for 2 min then 6 °C/min to 310 °C, and then held for 15 min. Results are reported in delta notation (‰) and normalized to a suite of *n*-alkanes with a known isotopic composition (*n*-C<sub>16</sub> to *n*-C<sub>30</sub>; i.e., the A7 standard reference material obtained from Arndt Schimmelmann). Standards were run in triplicate before and after each sample batch (*n* = 5). The standard deviation was typically between ~2 and 5‰. Samples were rejected when the standard deviation exceeded 5‰. Error bars represent the standard deviation of the A-7 mix run in concert with samples. The H<sub>3</sub><sup>+</sup> factor calculated prior to each sample sequence was consistently below 4 ppm V<sup>-1</sup>. Hydrogen isotopes are expressed relative to Vienna Standard Mean Ocean Water (VSMOW).

#### 2.4. Biomarker ratios

Several methods for characterising the *n*-alkane distribution of a sample have been developed, including the carbon preference index (CPI), average chain length (ACL) and odd-over-even predominance (OEP). In fresh plant material, the CPI is high (>5 to 40; Bush and McInerney, 2013), but decreases over time due to thermal maturation, approaching values of ~1 in mature oils and sediments. The CPI is calculated following Marzi et al. (1993) as:

$$\text{CPI} = \frac{(2 \times (C_{23} + C_{25} + C_{27} + C_{29}))}{(C_{22} + 2 \times (C_{24} + C_{26} + C_{28}) + C_{30})} \quad (1)$$

ACL represents the weighted averages of carbon chain lengths and can be calculated as (Ficken et al., 2000; Bush and McInerney, 2013):

$$\text{ACL} = \frac{((25 \times C_{25}) + (27 \times C_{27}) + (29 \times C_{29}) + (31 \times C_{31}) + (33 \times C_{33}))}{C_{25} + C_{27} + C_{29} + C_{31} + C_{33}} \quad (2)$$

Vascular plants synthesize hydrocarbons with a strong predominance of odd-over-even numbered *n*-alkanes. The formula to determine OEP used here (following Scalan and Smith, 1970) is:

$$\text{OEP} = \frac{(C_{27} + (6 \times C_{29}) + C_{31})}{((4 \times C_{28}) + (4 \times C_{30}))} \quad (3)$$

### 3. Results

#### 3.1. Leaf wax distributions

In the most distal site (Utah State 1), CPI values are relatively low and range from 1.4 and 2.4, with little observed variation apart from slight fluctuations towards the base and top of the Mahogany Zone. The P-4 core exhibits variable CPI values ranging from 0.7 to 3.5 with larger variations towards the base and top of the section. In the most proximal site (Skyline 16), CPI values are relatively high (1.9 to 4.5) with larger variations towards the base and top.

As expected, the OEP values for each site display similar patterns. In the most distal site (Utah State 1), the OEP ranges between 1.5 and 3.9. The P-4 core exhibits variable OEP values (ca. 0.5 to 10.6), with more variation at the base and top. In the most proximal site (Skyline 16), OEP values fluctuate from 4.1 up to 10.2, with higher values observed towards the upper and the lower portions of the Mahogany Zone.

In the most distal site (Utah State 1), the ACL is characterized by very similar values through the section (27.7 to 30.0), with stronger variation

in values towards the base and top of the section. ACL values in P-4 range from 26.3 to 30.8, with more variation observed in the deepest samples (781.7–763.15 ft). In the most proximal core (Skyline 16), ACL values vary from 28.5 to 30.2, showing minor variability with values slightly higher than those in the Utah State 1 and P-4 cores (Tables 1–3, see Supplementary Information).

#### 3.2. Compound-specific hydrogen isotope values

##### 3.2.1. Utah State 1

C<sub>29</sub> *n*-alkane  $\delta^2\text{H}$  ( $\delta^2\text{H}_{\text{wax}}$ ) values range from –111.2 to –169.4‰ (Fig. 2). The highest  $\delta^2\text{H}_{\text{wax}}$  values (–111.2‰) are found at 2371.5 ft. (correlating to the Curly Tuff bed, an ash layer deposited in a tuffaceous debris flow; Smith et al., 2008) and the lowest  $\delta^2\text{H}_{\text{wax}}$  values (–169.4‰) are found at 2290.15 ft.  $\delta^2\text{H}_{\text{wax}}$  values are particularly low at 2314.1 and 2311.45 ft. (–165.2 and –166.8‰ respectively) and represent beds that are rich in organic matter, including the Mahogany Bed at 2314 ft. Phytane  $\delta^2\text{H}$  ( $\delta^2\text{H}_{\text{phytane}}$ ) values range from –245.7 to –292.4‰, with the highest  $\delta^2\text{H}_{\text{phytane}}$  values present at the base of the section. Lower  $\delta^2\text{H}_{\text{phytane}}$  values are observed at 2314.1 and 2308.3 ft. (–289.6 and –291.4‰ respectively), coinciding with lower  $\delta^2\text{H}_{\text{wax}}$  values.

##### 3.2.2. P-4

$\delta^2\text{H}_{\text{wax}}$  values from the more proximal P-4 range from –89.4 to –143.0‰, which are higher than values in Utah State 1 and Skyline 16. Less variability is observed in this proximal core (typically  $\pm 10\%$ ) and no clear trend is observed upwards through the section. The lowest  $\delta^2\text{H}_{\text{wax}}$  value is seen at 731 ft. (–143.0‰) and the second lowest  $\delta^2\text{H}_{\text{wax}}$  value recorded is –110.1‰, immediately below the deposition of the Mahogany Bed. In the proximal P-4 core,  $\delta^2\text{H}_{\text{phytane}}$  values are relatively low and vary from –247.0 to –224.6‰. We observe an upwards trend of increasingly lower  $\delta^2\text{H}_{\text{phytane}}$  values in the middle and upper sections with higher  $\delta^2\text{H}_{\text{phytane}}$  values near the base (748.5–738.0 ft).

##### 3.2.3. Skyline 16

$\delta^2\text{H}_{\text{wax}}$  values in the Skyline 16 core vary from –164.1 to –208.5‰ (472.1 and 437.9 respectively). There is a trend of progressively lower  $\delta^2\text{H}$  values through the Mahogany Zone samples in Skyline 16.  $\delta^2\text{H}_{\text{phytane}}$  values in the Skyline 16 core vary from –295.6 to –265.4‰. Much of the section, however, shows much more limited variation. However, the top of section exhibits higher  $\delta^2\text{H}_{\text{phytane}}$  values.

### 4. Discussion

#### 4.1. Controls on phytane $\delta^2\text{H}$ values within the Uinta Basin

The hydrogen isotopic composition of phytane is affected by multiple controls, including changes in source organism and/or variations in source water  $\delta^2\text{H}$ . These factors need to be considered before interpreting the isotopic record (see discussion below).

##### 4.1.1. Non-algal sources

Phytane is mostly derived from the side chain of chlorophyll-*a*. As such, it is thought to average the entire phytoplankton community (Witkowski et al., 2018). However, phytane can have multiple sources (e.g. methanogens and halophiles; ten Haven et al., 1987), which may influence  $\delta^2\text{H}_{\text{phytane}}$  values. We argue that inputs from methanogens and halophiles are relatively minor, due to the extreme productivity of the lake autotrophs within the photic zone and evidence for predominantly microbial organic matter found in petrographical studies (Elson et al., 2022). This would have vastly outweighed the potential input from these alternate sources.

##### 4.1.2. Changes in source water $\delta^2\text{H}$

The input of  $^2\text{H}$ -depleted snowmelt into the lake basin may affect  $\delta^2\text{H}_{\text{phytane}}$  values during the growing season. Early Paleogene

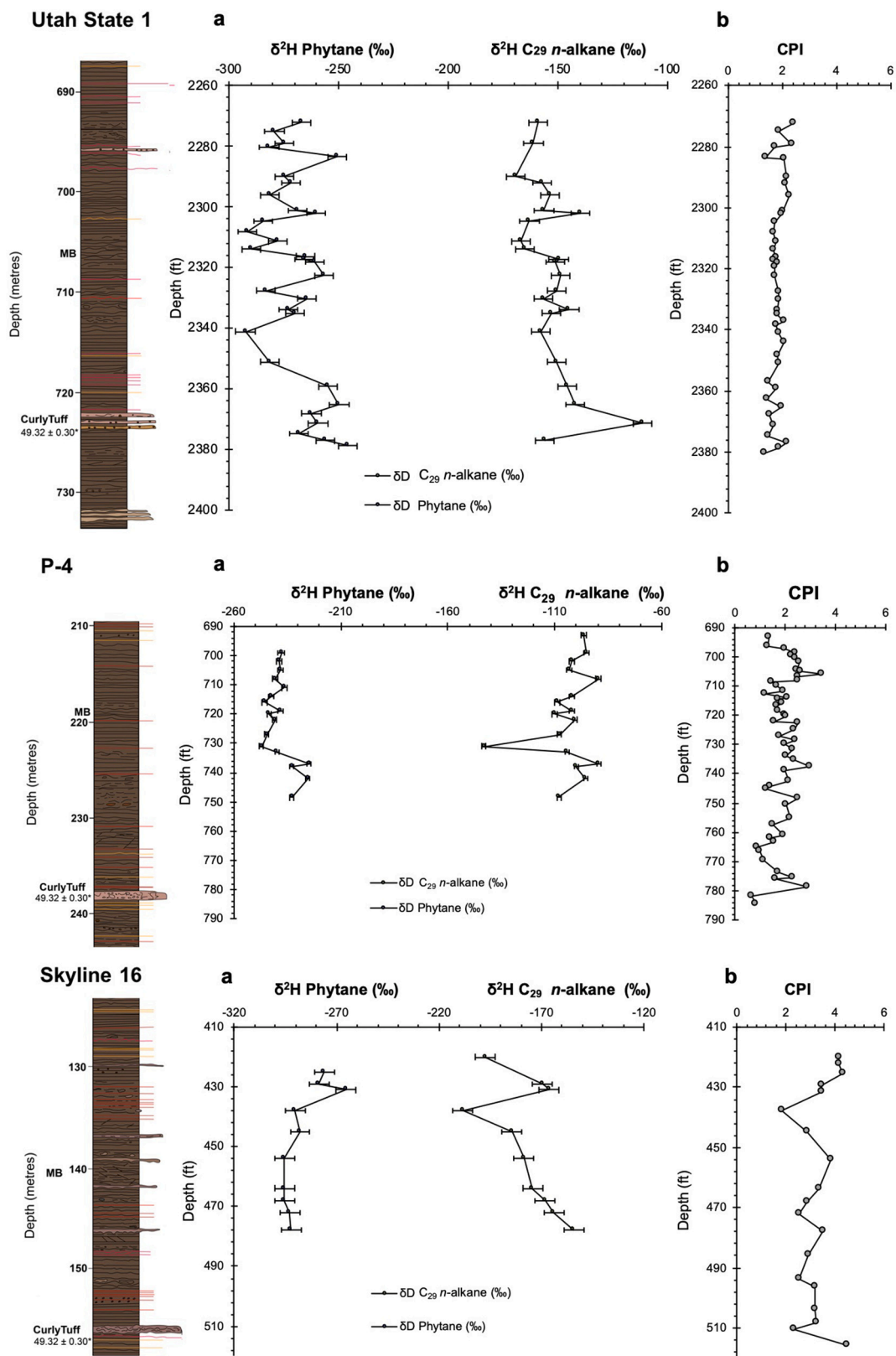


**Fig. 2.** (Top) Utah State 1 core results: Stratigraphic column through the Mahogany Zone, Utah State 1, through the basin center (a) Left:  $\delta^2\text{H}$  of phytane. Right:  $\delta^2\text{H}$  of C<sub>29</sub> n-alkane. (b) CPI measurements with higher values indicating an increased input of vascular plant material (calculated from Marzi et al., 1993.) (Middle) P-4 core results: Stratigraphic column through the Mahogany Zone, P-4, through the basin margin (a) Left:  $\delta^2\text{H}$  of phytane and C<sub>29</sub> n-alkane. Right:  $\delta^2\text{H}$ . (b) CPI measurements. (Bottom) Skyline 16 core results: Stratigraphic column through the Mahogany Zone, Skyline 16, through the basin margin (a) Left:  $\delta^2\text{H}$  of phytane. Right:  $\delta^2\text{H}$  of C<sub>29</sub> n-alkane. (b) CPI measurements. MB = Mahogany Bed Marker. (\* Smith et al., 2008). Error bars represent 1 $\sigma$  uncertainties. Depth is reported in both meters (stratigraphic log) and feet (geochemical results).

topography reconstructed for the Uinta Mountains reached at least 3000 m high with a basin floor paleoelevation of, at most, 1000 m high (Gao and Fan, 2018) and may have supplied snowmelt to the surrounding lake basins (Norris et al., 1996; Sewall and Sloan, 2006). However, proxy estimates from the basin have placed mean annual air temperature (MAAT; Wing, 1998) and warm month mean temperature (WMMT) estimates at  $\sim 16$  °C and  $\sim 40$  °C (Snell et al., 2013), respectively. Combined with floral and faunal studies (Wing, 1998), this suggests that temperatures would rarely drop below zero. Well-preserved palm trees (e.g. *Phoenix windmillis*; Snell et al., 2013) and fossil crocodylians (Markwick, 1994), have also been found through the Green River Formation and wider region, indicating CMMT  $>5$  °C (cold month mean temperature) and MAT  $>10$  °C. Thus, it is unlikely that input of  $^2\text{H}$ -depleted snowmelt into the lake basin changed dramatically over our timescales (e.g.,  $\sim 10^3$ – $10^4$  kyrs).

The  $\delta^2\text{H}$  value of the lake surface water would have been particularly sensitive to water balance changes in the basin, either through precipitation-evaporation (P-E) and/or the addition of isotopically distinct water from other sources. Previous work in the Uinta Basin has identified three hypersaline zones within the upper Green River Formation (Vanden Berg and Birgenheier, 2017). The first of these hypersaline phases coincides with deposition of the Mahogany Zone and is restricted to the eastern side of the basin, where the depocenter of the lake was located. Drivers of hypersalinity have been attributed to the input of Lake Gosiute water and associated high-density brines from the Greater Green River Basin to the north, which was far more evaporitic in nature and was undergoing north-south infilling (Smith et al., 2008). Water transported to Lake Uinta from the shallower, evaporitic basin would have been  $^2\text{H}$ -enriched and associated with relatively high  $\delta^2\text{H}_{\text{phytane}}$  values (Fig. 5). Skyline 16 – which is further to the south-east and shallower than the other locations – has the lowest  $\delta^2\text{H}_{\text{phytane}}$  values and may have received less input of  $^2\text{H}$ -enriched water. The avulsion of river channels and adjustment of regional fluvial systems to a decreasingly energetic hydrological regime may have also resulted in different water sources being delivered to P-4 and Skyline 16, despite their relative proximity in location (Gall et al., 2017; Birgenheier et al., 2019). Although further work is required, it is likely that input of  $^2\text{H}$ -enriched, saline water exerted an important control on  $\delta^2\text{H}_{\text{phytane}}$  values in the hypersaline portions of the Uinta Basin.

#### 4.2. Controls on leaf wax $\delta^2\text{H}$ values within the Uinta Basin

$\delta^2\text{H}_{\text{wax}}$  values primarily reflect the  $\delta^2\text{H}$  value of the plant's source water and – by extension – the hydrogen isotopic composition of precipitation ( $\delta^2\text{H}_{\text{precip}}$ ; Sachse et al., 2012). However, a fractionation factor ( $\epsilon_{\text{precip}}$ ) is required to estimate  $\delta^2\text{H}_{\text{precip}}$ . Here we employ a net fractionation factor of  $110 \pm 20\%$  as this captures the variability in modern  $\text{C}_3$  gymnosperms and angiosperms (Sachse et al., 2012; Pedentchouk et al., 2008). This yields average  $\delta^2\text{H}_{\text{precip}}$  values of  $-43\%$  (Utah State 1),  $+7\%$  (P-4) and  $-67\%$  (Skyline 16). These values are  $^2\text{H}$ -enriched ( $\sim 30$  to  $100\%$ ), relative to modern values of  $-96$  to  $-100\%$  (Bowen and Revenaugh, 2003). This can be explained by two mechanisms. Firstly, in a warmer climate, warmer air temperatures will yield more  $^2\text{H}$ -enriched water vapor (a temperature effect) (Poulsen et al., 2007; Speelman et al., 2010). Secondly, in a warmer world, there will be decreased rainout efficiency in the subtropics, resulting in more  $^2\text{H}$ -enriched precipitation at the mid-to-high latitudes (e.g., Pagani et al., 2006; Speelman et al., 2010). However, there are large ( $\sim 50$  to  $75\%$ ) inter-site variations that suggest additional controls on  $\delta^2\text{H}_{\text{precip}}$  values (see below).

##### 4.2.1. Diagenesis

Hydrogen exchange processes can alter lipid  $\delta^2\text{H}$  values slowly over time and overprint the original environmental signature (Sessions et al., 2004). The most common way to assess isotopic exchange is to compare long-chain *n*-alkane and isoprenoid (e.g. phytane)  $\delta^2\text{H}$  values

(Pedentchouk et al., 2006). In immature modern sediment samples, isoprenoids (e.g. phytol) are  $^2\text{H}$ -depleted (up to 150 to 200‰) relative to long-chain *n*-alkanes (Li et al., 2009). However, with increasing maturation, the offset between isoprenoids and long-chain *n*-alkanes diminishes to zero (Sessions, 2016 and references therein). In the Uinta Basin, the offset between isoprenoids (phytane) and *n*-alkanes is consistent and large ( $\sim 100$  to  $140\%$ ; Fig. 3), suggesting minimal hydrogen exchange. The Green River Formation is also known for the thermal immaturity of its vast oil shale resources (Birgenheier and Vanden Berg, 2011). Relatively low thermal maturity is supported by relatively high OEP ( $>4.1$  to 10.4) and relatively high CPI values ( $>1.5$ –4) recorded through the Mahogany Zone. Overall, this suggests that the impact of thermal maturity on  $\delta^2\text{H}$  values is minimal.

##### 4.2.2. Plant type

Changes in the plant community can influence the apparent fractionation between  $\delta^2\text{H}_{\text{wax}}$  and  $\delta^2\text{H}_{\text{precip}}$  values ( $\epsilon_{\text{precip}}$ ). In modern  $\text{C}_3$  plants,  $\epsilon_{\text{precip}}$  values range between ca.  $-80$  to  $-150\%$  (Sachse et al., 2012 and references therein) however, accounting for changes in plant community in ancient settings is challenging (Feakins, 2013). Recent work has used pollen assemblages to calculate plant-specific fractionation factors (e.g. Feakins, 2013; Inglis et al., 2022). However, this was not possible here because of the very high content of amorphous organic matter (AOM) in the samples. By volume this comprises the bulk of the samples so that any attempt to dissolve the sample in hydrochloric acid (HCl) or hydrofluoric acid (HF) is near impossible. The AOM both shields the mineral content which is also not sufficiently abundant that removing it disaggregates the sample to release the palynomorphs. An attempt was made to disaggregate the AOM with a tunable ultrasonic probe after the HF treatment but this had little effect. Alternatively, a shift in the average chain length (ACL) could potentially reveal a change in the higher plant community, as shown during the PETM (e.g. Schouten et al., 2007). Although modern plant surveys cast doubt as to whether the ACL can discriminate between key plant types (with the exception of mosses; Bush and McInerney, 2013), invariant ACL values in the Uinta Basin sediments imply no significant change in vegetation during the EECO.

##### 4.2.3. Soil and/or leaf water $^2\text{H}$ -enrichment

In modern sediments,  $\delta^2\text{H}_{\text{wax}}$  values are correlated with source water  $\delta^2\text{H}$  (i.e., precipitation). However, evaporative  $^2\text{H}$ -enrichment of soil and/or leaf water can modify  $\delta^2\text{H}_{\text{wax}}$  values, especially in (semi-)arid settings (Kahmen et al., 2012). Subsequently, the isotopic difference between terrestrial and aquatic biomarkers can be used to constrain soil and/or leaf water evaporative enrichment (see Rach et al., 2017 and references therein) and is typically calculated using long-chain *n*-alkanes ( $\text{C}_{29}$ – $\text{C}_{33}$ ; i.e. higher plants) and mid-chain *n*-alkanes ( $\text{C}_{21}$ – $\text{C}_{25}$ ; i.e. submerged macrophytes). However, other algal biomarkers (e.g. phytane) can be used (Rach et al., 2017). In sites where evaporative  $^2\text{H}$ -enrichment of soil and/or leaf water is minimal, there should be a linear relationship between  $\delta^2\text{H}_{\text{wax}}$  and  $\delta^2\text{H}_{\text{phytane}}$ . With increasing evaporative  $^2\text{H}$ -enrichment of soil and/or leaf, the relationship between  $\delta^2\text{H}_{\text{wax}}$  and  $\delta^2\text{H}_{\text{phytane}}$  will weaken. In the Uinta Basin, we find a significant positive linear relationship between  $\delta^2\text{H}_{\text{wax}}$  and  $\delta^2\text{H}_{\text{phytane}}$  ( $r^2 = 0.78$ ;  $p < 0.001$ ). This suggests minimal evaporative  $^2\text{H}$ -enrichment of soil and/or leaf water within the Uinta Basin (Fig. 4).

##### 4.2.4. Orogenic effects

Intercontinental basins are particularly sensitive to tectonic controls that can have numerous consequences for basin accommodation, sediment supply and lake stratification (Carroll and Bohacs, 1999). Tectonic upheaval leading to rising regional land elevation and dropping temperatures may result in more  $^2\text{H}$ -depleted precipitation being delivered to the basin (c.f., Dansgaard, 1964; Sachse et al., 2012).

During deposition of the Green River Formation, steady subsidence of the Uinta Basin increased accommodation space, while the sediment

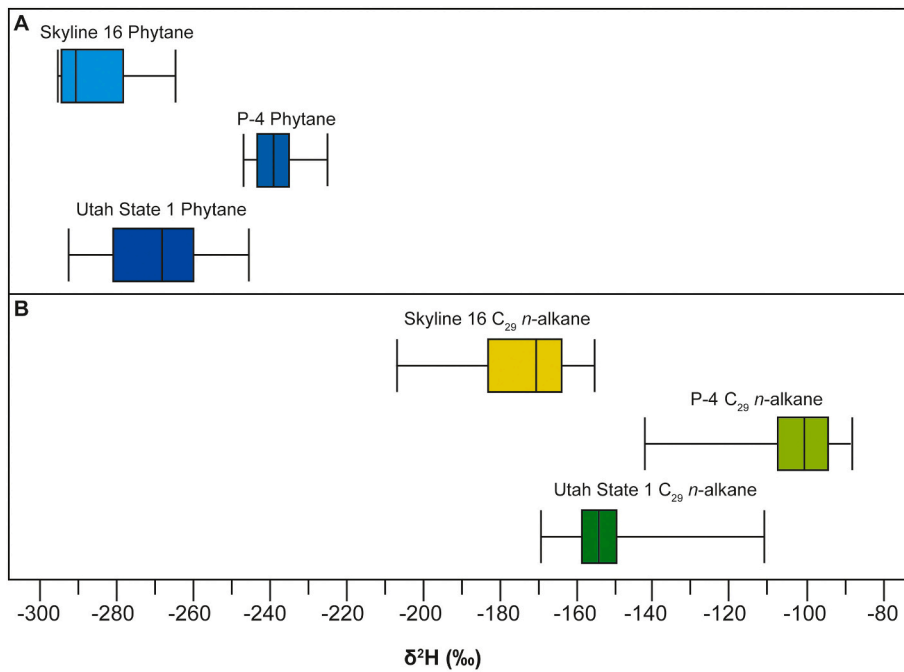


**Fig. 3.** Hydrogen isotope distributions of (a) phytane and (b)  $C_{29}$   $n$ -alkanes generated from three different sites in the Uinta Basin. Phytane  $\delta^2H$  values are consistently more negative relative to long-chain  $n$ -alkanes, primarily due to the different biosynthetic pathways. Large inter-site variations in phytane and  $n$ -alkanes are the result of strong  $\delta^2H$  controls via local processes. Whiskers represent highest and lowest values, and the box indicates the position of the upper quartile, mean and lower quartile for each set of results.

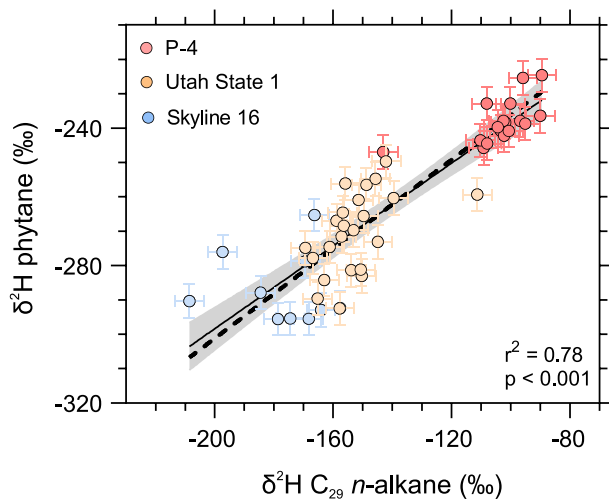


**Fig. 4.** Co-variation of phytane- and  $C_{29}$   $n$ -alkane  $\delta^2H$  values within early Eocene Uinta Basin sediments together with a Deming regression (dashed line) and simple linear regression (solid line). Also shown are the 95% confidence interval for the simple linear regression.

supply fluctuated, often paced by the Eocene hyperthermals (Gall et al., 2017). At the time of deposition of the Mahogany Zone, this long-term tectonic subsidence continued as a result of flexure from Laramide uplifts, including the Uinta Mountains towards the north and the Uncompahgre Uplift and San Rafael Swell towards the south. Paleocurrent data suggest the Douglas Creek Arch, a key structural high controlling connectivity between the Uinta and Piceance Creek basins, was uplifted during the Sunnyside Delta interval of the middle Green River Formation and prior to Mahogany Zone deposition (Birgenheier et al., 2019). In addition to the relatively short time span studied and the presence of several topographic highs surrounding the Uinta Basin, it is unlikely that changes in tectonic upheaval, resulting in a potential amount effect (Dansgaard, 1964) was a driver for the minor upwards depletion of  $\delta^2H$  observed in this section. However, at higher elevation, precipitation becomes progressively  $^2H$ -depleted (e.g., Bai et al., 2015). As such,

variations in  $\delta^2H_{wax}$  may be due to changes in plant wax source regions (e.g., low vs. high elevation).

#### 4.3. Stable hydrological cycle promoted OC burial during the EECO

Our leaf wax and phytane  $\delta^2H$  data indicate relatively gradual changes in source water  $\delta^2H$  in the Uinta Basin during deposition of the Mahogany Zone. This could indicate a stable hydrological cycle during the latter stages of the EECO, which differs from the more variable and dynamic hydrologic response observed during transient climatic events in the region, i.e., the PETM and early Eocene hyperthermals (Hyland et al., 2018). The latter are associated with high seasonality and ephemeral fluvial discharge, leading to high siliciclastic inputs (Gall et al., 2017; Birgenheier et al., 2019), whereas the EECO is characterized by the low siliciclastic input and a lower energy highstand lake (Gall et al., 2017; Birgenheier et al., 2019).

Reduced siliciclastic input during the EECO would have also limited dilution from inorganic (clastic) sediments and thus promoted rich organic matter accumulation within the lake. Indeed, the hyperthermal phase lacks evidence for OC-rich deposits (Birgenheier et al., 2019). Collectively, this suggests that during the termination of the EECO, the development of a stable hydrological cycle may have been critical to the development of the OC-rich (>35%) Mahogany Zone (~49.3 to 48.7 Ma). These large highly productive saline lakes possibly acted as carbon sinks, providing a negative climate feedback mechanism during intervals between hyperthermals (Birgenheier et al., 2019).

Intriguingly, the deposition of the Mahogany Zone is roughly coincident with the onset of long-term Eocene cooling (~48–49 Ma; Inglis et al., 2015; Smith et al., 2010; Gall et al., 2017). Large amounts of organic carbon would have been sequestered in Lake Uinta (~76 Gt; Elson et al., 2022), similar to the OC-rich (>5 wt%) deposition observed in deposits from the same time period in the High Arctic (Brinkhuis et al., 2006) and Nordic Seas (Brinkhuis et al., 2006; Barke et al., 2012). This suggests a link between carbon cycling and global climate evolution. Unlike the Uinta Basin, the high Arctic is characterized by low salinity conditions. However, both are strongly stratified, largely anoxic basins (Brinkhuis et al., 2006; Vanden Berg and Birgenheier, 2017) characterized by limited siliciclastic input (Birgenheier et al., 2019). Both suggest a stable hydrological cycle during the EECO and imply a

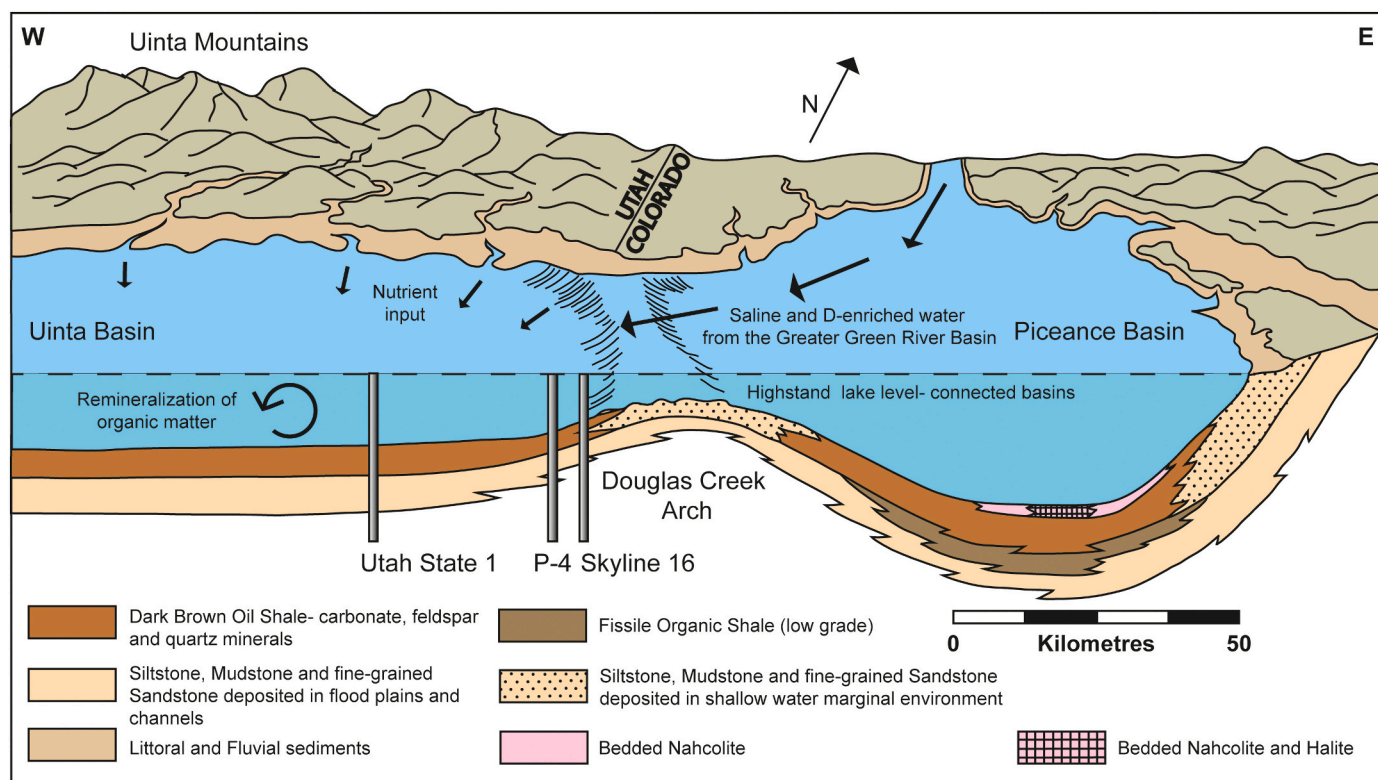


**Fig. 5.** The Uinta and Piceance basins connected by Lake Uinta at highstand, with locations of the basinal Utah State 1, proximally-located P-4 and the shallowest core, Skyline 16. Saline-rich and isotopically heavy  $^2\text{H}$  water originating in the Greater Green River Basin (Fig. 1) was transported into the connected Piceance Basin and over the submerged Douglas Creek Arch, into the Uinta Basin, spatially affecting source water for the algal lipids in the paleolake Uinta (Adapted from Dyni, 1987). (For interpretation of the references to colour in this figure legend, the reader is referred to the web version of this article.)

causal relationship between the hydrological cycle, organic matter burial and carbon cycling during the early Eocene. However, additional work from other sites is required to test this hypothesis.

## 5. Conclusions

Here we use leaf wax and algal lipid  $\delta^2\text{H}$  analysis to study the hydrological regime in the mid-latitude continental interior during the latest EECO and post-EECO interval (~49.3 to 48.7 Ma). We find large inter-site variation in both leaf wax and algal lipid  $\delta^2\text{H}$  values. This may have arisen from various factors, including the input of  $^2\text{H}$ -enriched, saline water from Lake Gosiute. Unlike the more variable hydrological regime of the early Eocene hyperthermals, limited variations in  $\delta^2\text{H}$  values during the deposition of the Mahogany Zone suggest a relatively stable hydrological cycle during the latest EECO. We interpret this to indicate that the hydrologic cycle responds differently during rapid vs. gradual climatic perturbations. A stable hydrological regime may provide conditions that promote organic matter productivity and preservation within large lacustrine systems and may serve as an important negative climatic feedback during intervals of sustained global warmth.

## Declaration of Competing Interest

The authors declare that they have no known competing financial interests or personal relationships that could have appeared to influence the work reported in this paper.

## Acknowledgements

This contribution represents a portion of A. Elson's doctoral dissertation at the University of Southampton, funded by the Natural Environment Research Council Centre for Doctoral Training in Oil & Gas.

Oliver Bench assisted with field work and sample collection and P. Sargent Bray is acknowledged for help with organic geochemistry. Discussions with Mike Vanden Berg contributed to the development of this manuscript. Funding was provided by CASP and the NSF for fieldwork and workshop attendance for A. Elson, and the Donors to the Petroleum Research Fund of the American Chemical Society to J. H. Whiteside. G. N-Inglis was funded by a GCRF Royal Society Dorothy Hodgkin Fellowship (DHF/R1\191178).

## Appendix A. Supplementary data

Supplementary data to this article can be found online at <https://doi.org/10.1016/j.palaeo.2022.110959>.

## References

- Bai Dr, Y, Fang Dr, X, Jia Dr, G, Sun Dr, J, Wen Dr, R, Ye Dr, Y, et al., 2015. Different altitude effect of leaf wax n-alkane  $\delta\text{D}$  values in surface soils along two vapor transport pathways, southeastern Tibetan Plateau. *Geochimica et Cosmochimica Acta* 170, 94–107.
- Barke, J., van der Burgh, J., van Konijnenburg-van Cittert, J.H.A., Collinson, M.E., Pearce, M.A., Bujak, J., Heilmann-Clausen, C., Speelman, E.N., van Kempen, M.M.L., Reichart, G., Lotter, A.F., Brinkhuis, H., 2012. Coeval Eocene blooms of the freshwater fern *Azolla* in and around Arctic and Nordic seas. *Palaeogeogr. Palaeoclimatol. Palaeoecol.* 337–338, 108–119. <https://doi.org/10.1016/j.palaeo.2012.04.002>.
- Birgenheier, L.P., Vanden Berg, M.D., 2011. Core-based integrated sedimentologic, stratigraphic, and geochemical analysis of the oil shale bearing Green River Formation, Uinta Basin, Utah. In: University of Utah Institute for Clean and Secure Energy, United States Department of Energy. Oil & Natural Gas Technology Technical Report, vol. 19.
- Birgenheier, L.P., Vanden Berg, M.D., Plink-Björklund, P., Gall, R.D., Rosencrans, E., Rosenberg, M.J., Toms, L.C., Morris, J., 2019. Climate impact on fluvial-lake system evolution, Eocene Green River Formation, Uinta Basin, Utah, USA. *Geol. Soc. Am. Bull.* 132, 562–587.
- Bowen, G.J., Revenaugh, J., 2003. Interpolating the isotopic composition of modern meteoric precipitation. *Water Resour. Res.* 39 (10).

- Bradley, W.H., 1929. The varves and climate of the Green River epoch. In: U.S. Geological Survey Professional Paper 158-E.
- Brinkhuis, H., Schouten, S., Collinson, M.E., Sluijs, A., Damsté, J.S.S., Dickens, G.R., Huber, M., Cronin, T.M., Onodera, J., Takahashi, K., Bujak, J.P., 2006. Episodic fresh surface waters in the Eocene Arctic Ocean. *Nature* 441 (7093), 606–609.
- Bush, R.T., McInerney, F.A., 2013. Leaf wax *n*-alkane distributions in and across modern plants: implications for paleoecology and chemotaxonomy. *Geochim. Cosmochim. Acta* 117, 161–179.
- Carmichael, M.J., Lunt, D.J., Huber, M., Heinemann, M., Kiehl, J., LeGrande, A., Loftson, C.A., Roberts, C.D., Sagoo, N., Shields, C., Valdes, P.J., 2016. A model–model and data–model comparison for the early Eocene hydrological cycle. *Clim. Past* 12 (2), 455–481.
- Carmichael, M.J., Inglis, G.N., Badger, M.P., Naafs, B.D.A., Behrooz, L., Rimmelzwaal, S., Monteiro, F.M., Rohrsen, M., Farnsworth, A., Buss, H.L., Dickson, A.J., 2017. Hydrological and associated biogeochemical consequences of rapid global warming during the Paleocene-Eocene Thermal Maximum. *Glob. Planet. Chang.* 157, 114–138.
- Carroll Dr, Alan, Bohacs Dr, Kevin, 1999. Stratigraphic classification of ancient lakes: Balancing tectonic and climatic controls. *Geology* 27 (2), 99–102.
- Dansgaard, W., 1964. Stable isotopes in precipitation. *Tellus* 16 (4), 436–468.
- Dyni, J.R., 1987. The origin of oil shale and associated minerals. In: Taylor, O.J. (Ed.), *Oil Shale, Water Resources, and Valuable Minerals of the Piceance Basin, Colorado - The Challenge and Choices of Development*. U.S. Geological Survey Professional Paper, 1310, pp. 17–20.
- Eglinton, T.I., Eglinton, G., 2008. Hydrogen isotope fractionation during water uptake by woody xerophytes. *Molecular proxies for paleoclimatology. Earth Planet. Sci. Lett.* 275, 1–16.
- Elson, A.L., Marshall, J.E., Whiteside, J.H., 2022. Controls on organic matter variation during deposition of the Mahogany Oil Shale Zone of the Parachute Creek Member, Green River Formation, Utah. In: *The Lacustrine Green River Formation: Hydrocarbon Potential and Eocene Climate Record*. UGA-51. Utah Geological Association Guidebook.
- Feakins, S.J., 2013. Pollen-corrected leaf wax D/H reconstructions of northeast African hydrological changes during the late Miocene. *Palaeogeogr. Palaeoclimatol. Palaeoecol.* 374, 62–71.
- Ficken, K.J., Li, B., Swain, D., Eglinton, G., 2000. An *n*-alkane proxy for the sedimentary input of submerged/floating freshwater aquatic macrophytes. *Org. Geochem.* 31, 745–749.
- Gall, R.D., Birgenheier, L.P., Vanden Berg, M.D., 2017. Highly seasonal and perennial fluvial facies: implications for climate control on the Douglas Creek and Parachute Creek members, Green River Formation, Southeastern Uinta Basin, Utah, U.S.A. *J. Sediment. Res.* 87 (9), 1019–1047. <https://doi.org/10.2110/jsr.2017.54>.
- Gao, M., Fan, M., 2018. Depositional environment, sediment provenance and oxygen isotope paleoaltimetry of the early Paleogene greater Green River Basin, southwestern Wyoming, USA. *Am. J. Sci.* 318 (10), 1018–1055.
- Grande, L., 1984. Paleontology of the Green River Formation, with a review of the fish fauna. *Bull. Geol. Surv. Wyoming* 64, 333.
- Hyland, E.G., Sheldon, N.D., 2013. Coupled CO<sub>2</sub>-climate response during the early Eocene climatic optimum. *Palaeogeogr. Palaeoclimatol. Palaeoecol.* 369, 125–135.
- Hyland, E.G., Huntington, K.W., Sheldon, N.D., Reichgelt, T., 2018. Temperature seasonality in the North American continental interior during the Early Eocene Climatic Optimum. *Clim. Past* 14 (10), 1391–1404.
- Inglis, G.N., Farnsworth, A., Lunt, D.J., Foster, G.L., Hollis, C.J., Pagani, M., Jardine, P.E., Pearson, P.N., Markwick, P., Galsworthy, A.M., Raynham, L., 2015. Descent toward the Icehouse: Eocene Sea surface cooling inferred from GDGT distributions. *Paleoceanography* 30 (7), 1000–1020.
- Inglis, G.N., Bragg, F., Burls, N.J., Cramwinckel, M.J., Evans, D., Foster, G.L., Huber, M., Lunt, D.J., Siler, N., Steinig, S., Tierney, J.E., Wilkinson, R., Anagnostou, E., de Boer, A.M., Dunkley Jones, T., Edgar, K.M., Hollis, C.J., Hutchinson, D.K., Pancost, R.D., 2020. Global mean surface temperature and climate sensitivity of the early Eocene Climatic Optimum (EECO), Paleocene–Eocene Thermal Maximum (PETM), and latest Paleocene. *Clim. Past* 16, 1953–1968. <https://doi.org/10.5194/cp-16-1953-2020>.
- Inglis, G.N., Toney, J.L., Zhu, J., Poulsen, C.J., Röhl, U., Jamieson, S.S., Pross, J., Cramwinckel, M., Krishnan, S., Pagani, M., Bijl, P.K., 2022. Enhanced terrestrial carbon export from East Antarctica during the early Eocene. *Paleoceanogr. Palaeoclimatol.* 37 (2), 1–14. [p.e2021PA004348](https://doi.org/10.2110/jsr.2020.24).
- Kahmen, A., Schefuss, E., Arndt, S.K., Hoffmann, B., Cernusak, L.A., West, J.B., Sachse, D., 2012. Leaf wax *n*-alkane  $\delta$ D values as ecohydrological proxies that reflect the  $\delta$ D values of precipitation and leaf water evaporative deuterium enrichment. In: *AGU Fall Meeting Abstracts*. 2012, B33A-0510.
- Li, C., Sessions, A.L., Kinnaman, F.S., Valentine, D.L., 2009. Hydrogen-isotopic variability in lipids from Santa Barbara Basin sediments. *Geochim. Cosmochim. Acta* 73 (16), 4803–4823.
- Markwick, P.J., 1994. "Equability," continentality, and Tertiary" climate": the crocodilian perspective. *Geology* 22 (7), 613–616.
- Marzi, R., Torkelson, B.E., Olson, R.K., 1993. A revised carbon preference index. *Org. Geochem.* 20 (8), 1303–1306.
- Norris, R.D., Jones, L.S., Corfield, R.M., Carlidge, J.E., 1996. Skiing in the Eocene Uinta Mountains? Isotopic evidence in the Green River Formation for snow melt and large mountains. *Geology* 24 (5), 403–406. [https://doi.org/10.1130/0091-7613\(1996\)024](https://doi.org/10.1130/0091-7613(1996)024).
- Pagani, M., Pedentchouk, N., Huber, M., Sluijs, A., Schouten, S., Brinkhuis, H., Sinninghe Damsté, J.S., Dickens, G.R., 2006. Arctic hydrology during global warming at the Paleocene/Eocene thermal maximum. *Nature* 442 (7103), 671–675.
- Pedentchouk, N., Freeman, K.H., Harris, N.B., 2006. Different response of  $\delta$ D values of *n*-alkanes, isoprenoids, and kerogen during thermal maturation. *Geochim. Cosmochim. Acta* 70 (8), 2063–2072. <https://doi.org/10.1016/j.gca.2006.01.013>.
- Pedentchouk, N., Sumner, W., Tipple, B., Pagani, M., 2008.  $\delta$ 13C and  $\delta$ D compositions of *n*-alkanes from modern angiosperms and conifers: an experimental set up in Central Washington State, USA. *Org. Geochem.* 39 (8), 1066–1071.
- Poulsen, C.J., Pollard, D., White, T.S., 2007. General circulation model simulation of the  $\delta$ 18O content of continental precipitation in the middle Cretaceous: a model-proxy comparison. *Geology* 35 (3), 199–202.
- Rach, O., Kahmen, A., Brauer, A., Sachse, D., 2017. A dual-biomarker approach for quantification of changes in relative humidity from sedimentary lipid D/ H ratios. *Clim. Past* 13 (7), 741–757.
- Sachse, D., Radke, J., Gleixner, G., 2004. Hydrogen isotope ratios of recent lacustrine sedimentary *n*-alkanes record modern climate variability. *Geochim. Cosmochim. Acta* 68 (23), 4877–4889.
- Sachse, D., Billault, I., Bowen, G.J., Chikaraishi, Y., Dawson, T.E., Feakins, S.J., Freeman, K.H., Magill, C.R., McInerney, F.A., Van Der Meer, M.T., Polissar, P., 2012. Molecular paleohydrology: interpreting the hydrogen-isotopic composition of lipid biomarkers from photosynthesizing organisms. *Annu. Rev. Earth Planet. Sci.* 40, 221–249.
- Scalan, E.S., Smith, J.E., 1970. An improved measure of the odd-even predominance in the normal alkanes of sediment extracts and petroleum. *Geochim. Cosmochim. Acta* 34 (5), 611–620. [https://doi.org/10.1016/0016-7037\(70\)90019-0](https://doi.org/10.1016/0016-7037(70)90019-0).
- Schouten, S., Forster, A., Panot, F.E., Damsté, J.S.S., 2007. Towards calibration of the TEX<sup>86</sup> palaeothermometer for tropical sea surface temperatures in ancient greenhouse worlds. *Org. Geochem.* 38 (9), 1537–1546.
- Sessions, A.L., 2016. Factors controlling the deuterium contents of sedimentary hydrocarbons. *Org. Geochem.* 96, 43–64.
- Sessions, A.L., Slyva, S.P., Summons, R.E., Hayes, J.M., 2004. Isotopic exchange of carbon-bound hydrogen over geologic timescales. *Geochim. Cosmochim. Acta* 68 (7), 1545–1559. <https://doi.org/10.1016/j.gca.2003.06.004>.
- Sewall, J.O., Sloan, L.C., 2006. Come a little bit closer: a high-resolution climate study of the early Paleogene Laramide foreland. *Geology* 34 (2), 81–84.
- Smith, M.E., Carroll, A.R., Singer, B.S., 2008. Synoptic reconstruction of a major ancient lake system: Eocene Green River Formation, western United States. *Geol. Soc. Am. Bull.* 120, 54–84. <https://doi.org/10.1130/B26073.1>.
- Smith, M.E., Chamberlain, K.R., Singer, B.S., Carroll, A.R., 2010. Eocene clocks agree: coeval 40Ar/39Ar, U-Pb, and astronomical ages from the Green River Formation. *Geology* 38 (6), 527–530.
- Snell, K.E., Thrasher, B.L., Eiler, J.M., Koch, P.L., Sloan, L.C., Tabor, N.J., 2013. Hot summers in the Bighorn Basin during the early Paleogene. *Geology* 41 (1), 55–58.
- Speelman, E.N., Sewall, J.O., Noone, D., Huber, M., von der Heydt, A., Damsté, J.S., Reichart, G.J., 2010. Modeling the influence of a reduced equator-to-pole sea surface temperature gradient on the distribution of water isotopes in the Early/Middle Eocene. *Earth Planet. Sci. Lett.* 298 (1–2), 57–65.
- ten Haven, H.L., de Leeuw, J.W., Rullkötter, J., Sinninghe Damsté, J.S., 1987. Restricted utility of the pristane/phytane ratio as a paleoenvironmental indicator. *Nature* 330, 641–643.
- Tissot, B., Deroo, G., Hood, A., 1978. Geochemical study of the Uinta Basin: Formation of petroleum from the Green River Formation. *Geochim. Cosmochim. Acta* 42, 1469–1485.
- Vanden Berg, M.D., Birgenheier, L.P., 2017. An examination of the hypersaline phases of Eocene Lake Uinta, upper Green River Formation, Uinta Basin, Utah. *J. Paleolimnol.* 58, 353–371. <https://doi.org/10.1007/s10933-017-9983-x>.
- Volkman, J.K., Barrett, S.M., Blackburn, S.I., Mansour, M.P., Sikes, E.L., Gelin, F., 1998. Microalgal biomarkers: a review of recent research developments. *Org. Geochem.* 29, 1163–1179.
- Walters, A.P., Meyers, S.R., Carroll, A.R., Hill, T.R., Vanden Berg, M.D., 2020. Lacustrine cyclicity in the Early Eocene Green River Formation, Uinta Basin, Utah: evidence from X-ray fluorescence core scanning. *J. Sediment. Res.* 90, 429–447. <https://doi.org/10.2110/jsr.2020.24>.
- Whiteside, J.H., Van Keuren, M.A., 2009. Multiproxy environmental characterization of lake level cycles in the Green River Formation of Utah and Colorado. In: *Open-File Report 544*, Utah Geological Survey, 26.
- Wing, S.L., 1998. Late Paleogene–Early Eocene floral and climatic change in the Bighorn Basin, Wyoming. In: Aubry, M., Lucas, S., Berggren, W. (Eds.), *Late Paleocene–Early Eocene Climatic and Biotic Events in the Marine and Terrestrial Records*. Columbia University Press, New York, pp. 380–400.
- Witkowski, C.R., Weijers, J.W.H., Blais, B., Schouten, S., Sinninghe Damsté, J.S., 2018. Molecular fossils from phytoplankton reveal secular pCO<sub>2</sub> trend over the Phanerozoic. *Sci. Adv.* 4 eaat4556.
- Zachos, J.C., Pagani, M., Sloan, L., Thomas, E., Billups, K., 2001. Trends, rhythms, and aberrations in global climate 65 Ma to present. *Science* 292, 686–693. <https://doi.org/10.1126/science.1059412>.